CHAPTER 5

MECHANICAL AND ELECTROCHEMICAL BEHAVIOR OF ($Fe_{70}Ni_{30}$)-ZrO_2 METAL MATRIX COMPOSITES

Particle reinforced metal matrix composites are utilized for different engineering applications due to their better mechanical behavior as compared to the conventional materials. Different metal systems such as Fe, Ni, Co, Zn or their alloys (Fe-Zn, Ni-Fe, Fe-Co), etc. are used as a matrix phase for the fabrication of high strength metal matrix composites (MMCs). Of all these, Fe-Ni alloy system is a tough and durable material due to its high wear resistance and thermal stability. The presence of Ni also makes this alloy more corrosion resistant. The properties of metal matrix composites are availed by oxide dispersion strengthening. In this method, the addition of hard ceramic oxide particles such as Al_2O_3, ZrO_2, TiO_2, Y_2O_3, etc. are added in the metal or alloy matrix. The presence of these hard particles prevents the dislocation motion and grain boundary migration. The interaction between matrix and dispersed particles results in different specific characteristics.

Functional properties of the composite depend upon the composition, synthesis route, synthesis parameters, and microstructure. The dispersed particles must be uniformly distributed in the microstructure to avail the dispersion- hardening effect. Different processing routes such as hot pressing, plasma synthesis, casting, etc. are used for the metal matrix composite fabrication. Casting is also a good option for high-quality composite synthesis, but it is not suitable due to the high interfacial energy between the molten metal

and oxide particles. Therefore, powder metallurgy (P/M) route is an appropriate method for the materials having a high melting temperature. P/M route is also used due to unlimited compositional choices, homogeneity and low processing cost. It allows the composite to pass through some processing steps. These steps help in achieving the desired properties depending upon the application. It includes ball milling, compaction, and sintering as major steps. Ball milling as a part of P/M is used for synthesizing supersaturated solid solutions, nanocomposites, intermetallics, and dispersion strengthened materials. It is a nonequilibrium process where grain fragmentation results due to severe plastic deformation and this can be controlled by optimizing different processing parameters such as milling speed, milling duration, ball to powder ratio, etc. Further, the compaction and sintering of ball milled powders are essential steps to relax the nonequilibrium structure by releasing the extra strain energy at a higher temperature.

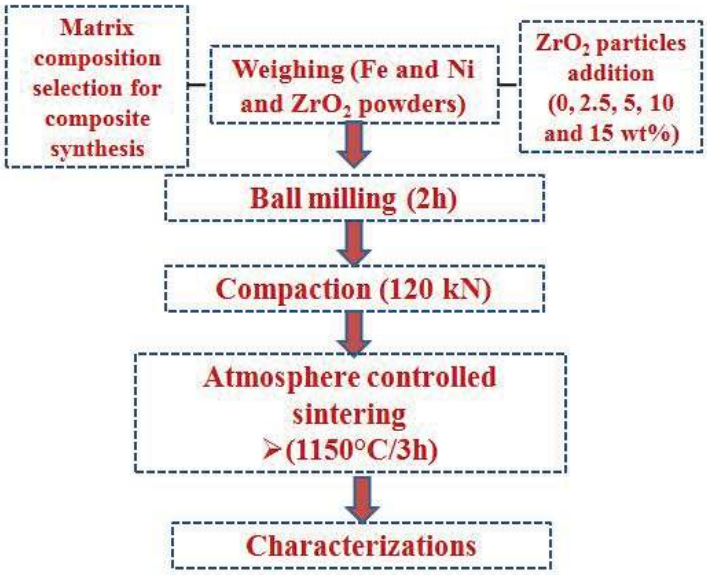

FIGURE 5.1: Synthesis flow diagram of (Fe-Ni)-ZrO_2 metal matrix composites.

In the previous chapter (Chapter 4), we have discussed the physical (phase, microstructure and density), mechanical (hardness and wear resistance) and electrochemical behavior (corrosion in 3.5 wt.% NaCl aqueous solution) of different $Fe_{(100-x)}Ni_{(x)}$ alloy specimens sintered at different temperatures. It was observed that increasing the Ni concentration in initial composition results in more γ-(Fe,Ni) phase formation, whereas α-(Fe,Ni) phase formation dominates at lower Ni content. These phases show a significant influence on all the physical, mechanical and electrochemical properties. At 30 wt.% Ni concentration, the wear resistance of the specimen was better than other compositions, and also the corrosion resistance was found to be improved. The $Fe_{70}Ni_{30}$ composition was selected for ZrO_2 particles dispersed metal matrix composite synthesis.

The present chapter describes the synthesis, physical, mechanical and corrosion behavior of (Fe,Ni)-ZrO_2 metal matrix composites. ZrO_2 is known for its very high hardness and high melting temperature as compared to many other oxide dispersions. In the present work, an effort has been made to disperse ZrO_2 (0, 2.5, 5, 10 and 15 wt.%) particles in $Fe_{70}Ni_{30}$ matrix composition. Five compositions named as ($Fe_{70}Ni_{30}$), ($Fe_{70}Ni_{30}$)-2.5ZrO_2, ($Fe_{70}Ni_{30}$)-5ZrO_2, ($Fe_{70}Ni_{30}$)-10ZrO_2 and ($Fe_{70}Ni_{30}$)-15ZrO_2 have been prepared by powder metallurgy and sintered at 1150°C/3h in atmosphere controlled furnace. The brief synthesis flow diagram for ($Fe_{70}Ni_{30}$)-ZrO_2 composites is shown in Fig. 5.1. The detailed discussion of synthesis and characterization is already provided in chapter 3.

Effect of ZrO_2 particles addition on the morphology of ball milled powder, and the phase formation, microstructure and mechanical behavior of sintered specimens has been studied. The effect of reinforcement concentration on the corrosion behavior in simulated

sea water environment (3.5 wt.% NaCl aqueous solution) is also focused. Chloride anion is the most common aggressive ion found in many industrial and natural environments. Iron-rich phase in $Fe_{70}Ni_{30}$ alloy system is susceptible to localized corrosion in chloride containing solutions. Therefore, ZrO_2 reinforcement has been done in $Fe_{70}Ni_{30}$ alloy composition to retard the attack of chloride ions.

5.1 X-ray Diffraction (XRD)

5.1.1 X-ray diffraction of ball milled powders

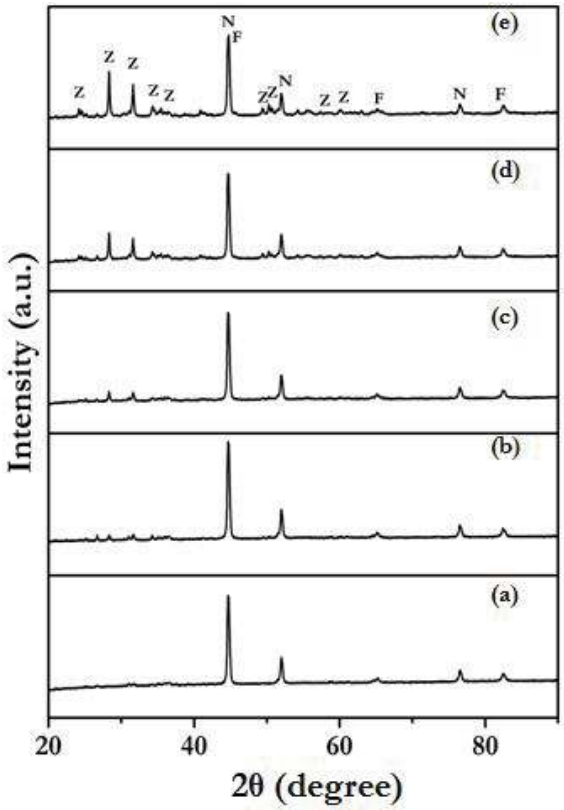

FIGURE 5.2: X-ray diffraction pattern of ball milled powders (a)($Fe_{70}Ni_{30}$) and (b)2.5 wt.% (c)5 wt.%, (d)10 wt.% (e)15 wt.% ZrO_2 reinforced ($Fe_{70}Ni_{30}$) (F- Fe; N- Ni and Z- ZrO_2).

Fig. 5.2 shows X-ray diffraction patterns of different ball milled powders. In the XRD pattern of ($Fe_{70}Ni_{30}$) ball milled powder with no ZrO_2 content, the presence of only Fe and Ni peaks is observed. In the remaining ball milled powders with ZrO_2 content as 2.5, 5, 10 and 15 wt.%, the presence of three different phases (Fe, Ni and ZrO_2) is observed. Observed phases are matched with the standard reference files of Fe (JCPDS-06-0696), Ni (JCPDS-04-0850) and monoclinic ZrO_2 (JCPDS-80-0966) which are distinguished in the plots. No intermediate phase formation between metal and ceramic phase has occurred during ball milling, and all the phases are found to be present as separate phases. As the concentration of Fe and Ni is constant in all the compositions, therefore, the peak intensity of Fe and Ni are similar in each plot. But as the concentration of ZrO_2 particles has increased from 0 to 15 wt.% in the milled powders, therefore, the peak intensity of monoclinic ZrO_2 phase in XRD pattern is increased with increasing ZrO_2 concentration. This is maximum in 15 wt.% ZrO_2 containing ball milled powder.

5.1.2 X-ray diffraction of sintered specimens

Fig. 5.3 shows the XRD patterns of the sintered composites (a)($Fe_{70}Ni_{30}$)-2.5ZrO_2 (b) ($Fe_{70}Ni_{30}$)-5ZrO_2 (c) ($Fe_{70}Ni_{30}$)-10ZrO_2 (d)($Fe_{70}Ni_{30}$)-15ZrO_2. From these patterns, phase formation in the synthesized specimens after sintering is determined. The presence of α-Fe (06-0696)/ α-(Fe,Ni) (37-0474); γ-(Fe,Ni) (47-1405) and ZrO_2 (80-0966) phases can be observed in the sintered specimens. It is interesting to note that Ni has formed a solid solution with Fe and formed γ-(Fe,Ni) and α-(Fe,Ni) alloy phases in ($Fe_{70}Ni_{30}$) matrix during sintering. The pattern of α-(Fe) and α-(Fe,Ni) overlap each other due to very

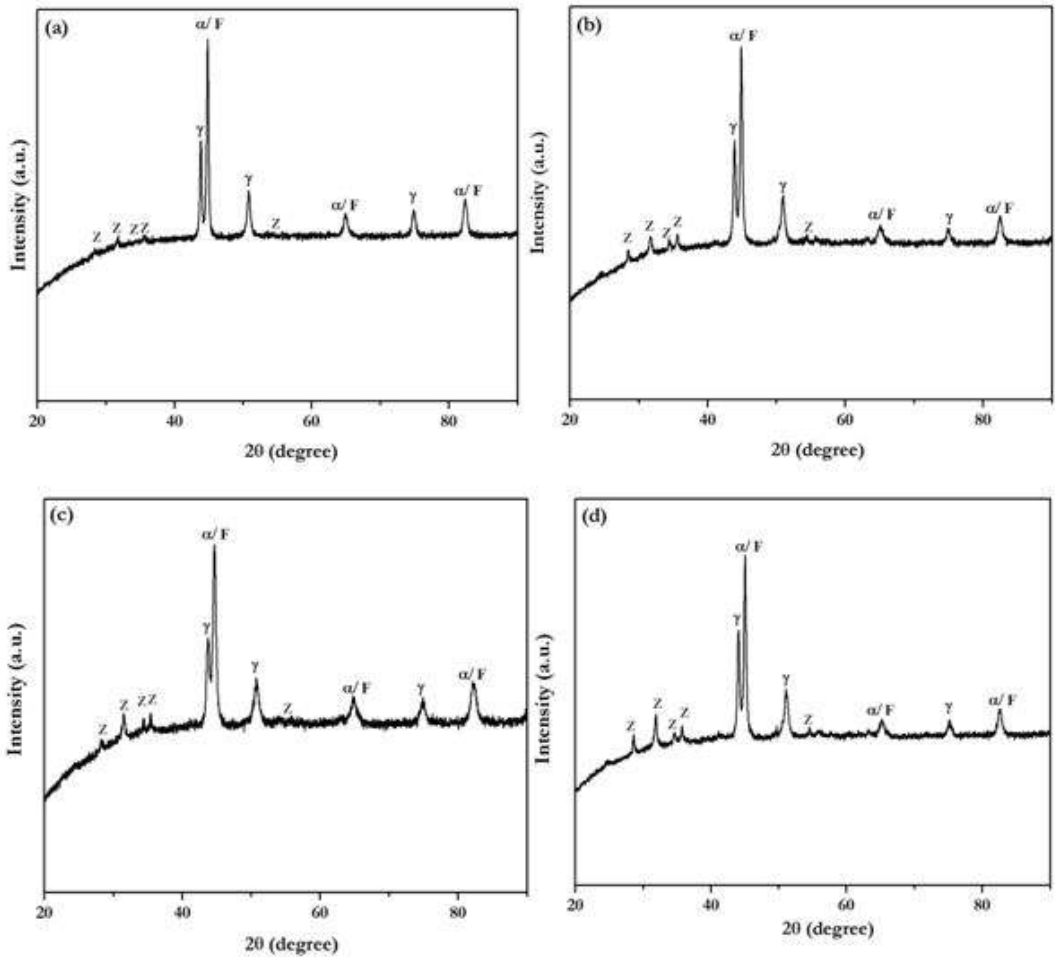

FIGURE 5.3: X-ray diffraction patterns of (a)($Fe_{70}Ni_{30}$) (b)($Fe_{70}Ni_{30}$)-2.5ZrO_2 (c)($Fe_{70}Ni_{30}$)-5ZrO_2 (d)($Fe_{70}Ni_{30}$)-10ZrO_2 (e)($Fe_{70}Ni_{30}$)-15ZrO_2 sintered composites. (F- Fe; α- α-(Fe,Ni); γ- γ-(Fe,Ni) and z- ZrO_2)

similar peak positions and crystal structure thus they are not easily distinguished. XRD patterns show distinct peaks of ceramic ZrO_2 reinforcement in ($Fe_{70}Ni_{30}$) matrix. The intensity of ZrO_2 peaks increases with increasing the wt. fraction of ZrO_2. It has been observed that ZrO_2 remains as a separate phase and there is no evidence of the reactive sintering or intermediate phase formation between metal and reinforcement phase. It is also observed that the peak intensity of γ-(Fe,Ni) phase has slightly increased, whereas the intensity of α-(Fe,Ni) phase has depressed with increasing the ZrO_2 content. This can

be concluded that ZrO_2 particles have contributed in reducing the particle size due to its high hardness during ball milling which increased the diffusion and enhanced γ-(Fe,Ni) phase formation.

5.2 Microstructure Evolution

5.2.1 Morphology of ZrO_2 raw powder and (Fe-Ni)-ZrO_2 ball milled powders

Fig. 5.4 shows the morphology of ZrO_2 powder used in the fabrication of (Fe,Ni)-ZrO_2 composites. The uniform ZrO_2 particles in round shapes can be observed in the micrograph.

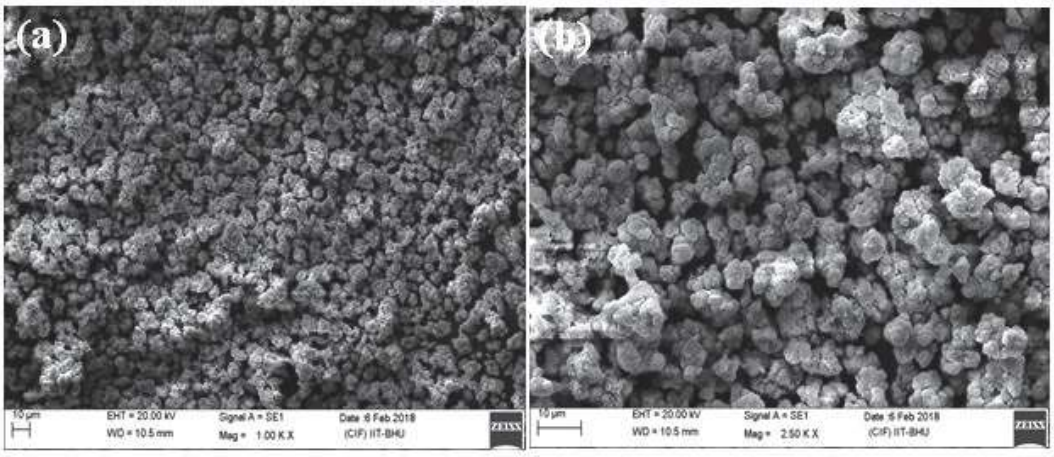

FIGURE 5.4: Scanning electron micrographs of ZrO_2 powder at (a) 1000x and (b) 2500x magnifications.

Figs. 5.5 and Fig. 5.6 show the SEM micrographs of (a)($Fe_{70}Ni_{30}$) (b)2.5 wt.% (c)5 wt.%, (d)10 wt.% and (e)15 wt.% ZrO_2 reinforced ($Fe_{70}Ni_{30}$) ball milled powders at 1000X and 10000X magnifications. It is observed from micrographs that the powders

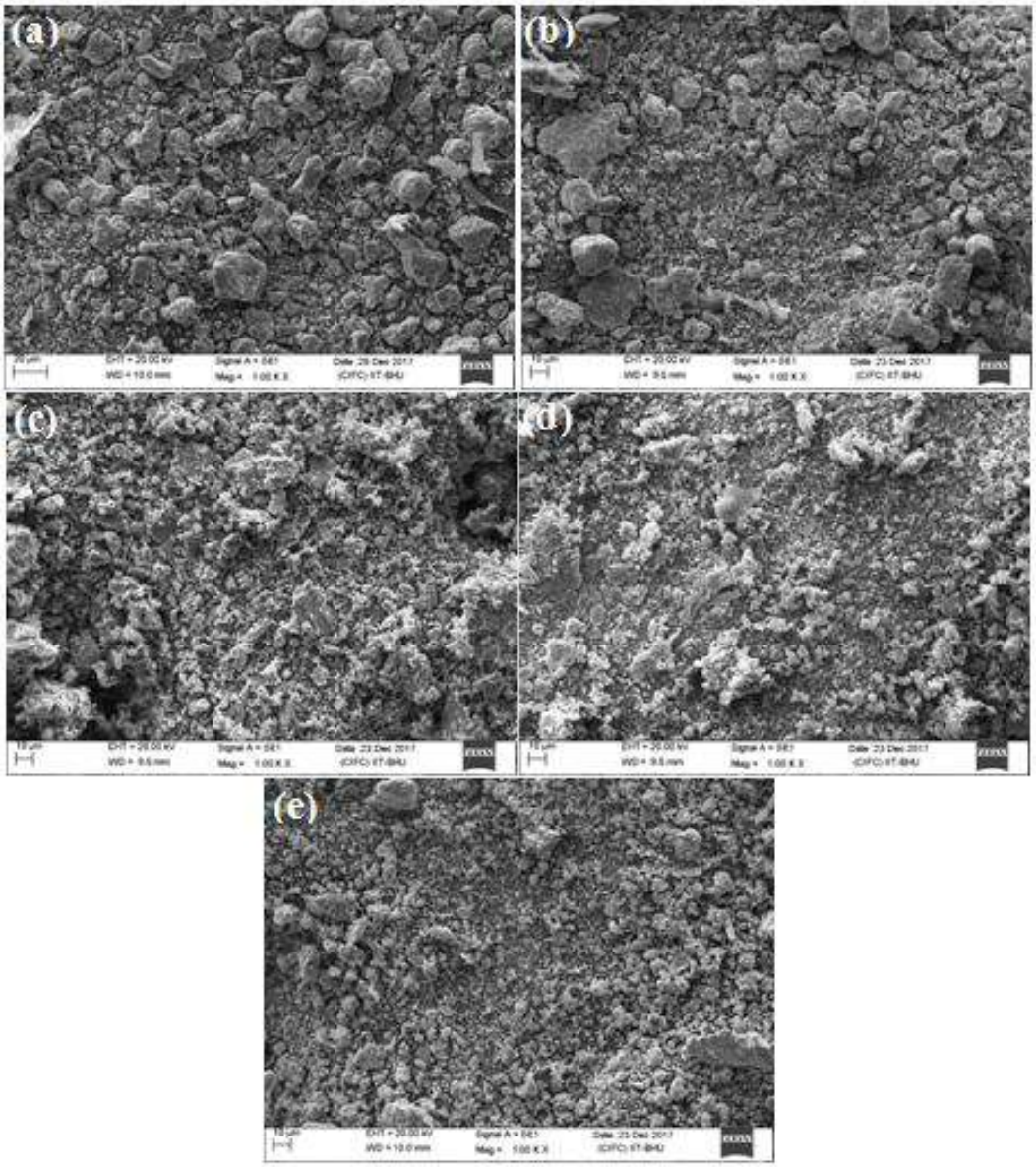

FIGURE 5.5: Scanning electron micrographs of (a)($Fe_{70}Ni_{30}$) (b)($Fe_{70}Ni_{30}$)-2.5ZrO_2 (c)($Fe_{70}Ni_{30}$)-5ZrO_2 (d)($Fe_{70}Ni_{30}$)-10ZrO_2 (e)($Fe_{70}Ni_{30}$)-15ZrO_2 ball milled powders at 1000X magnification.

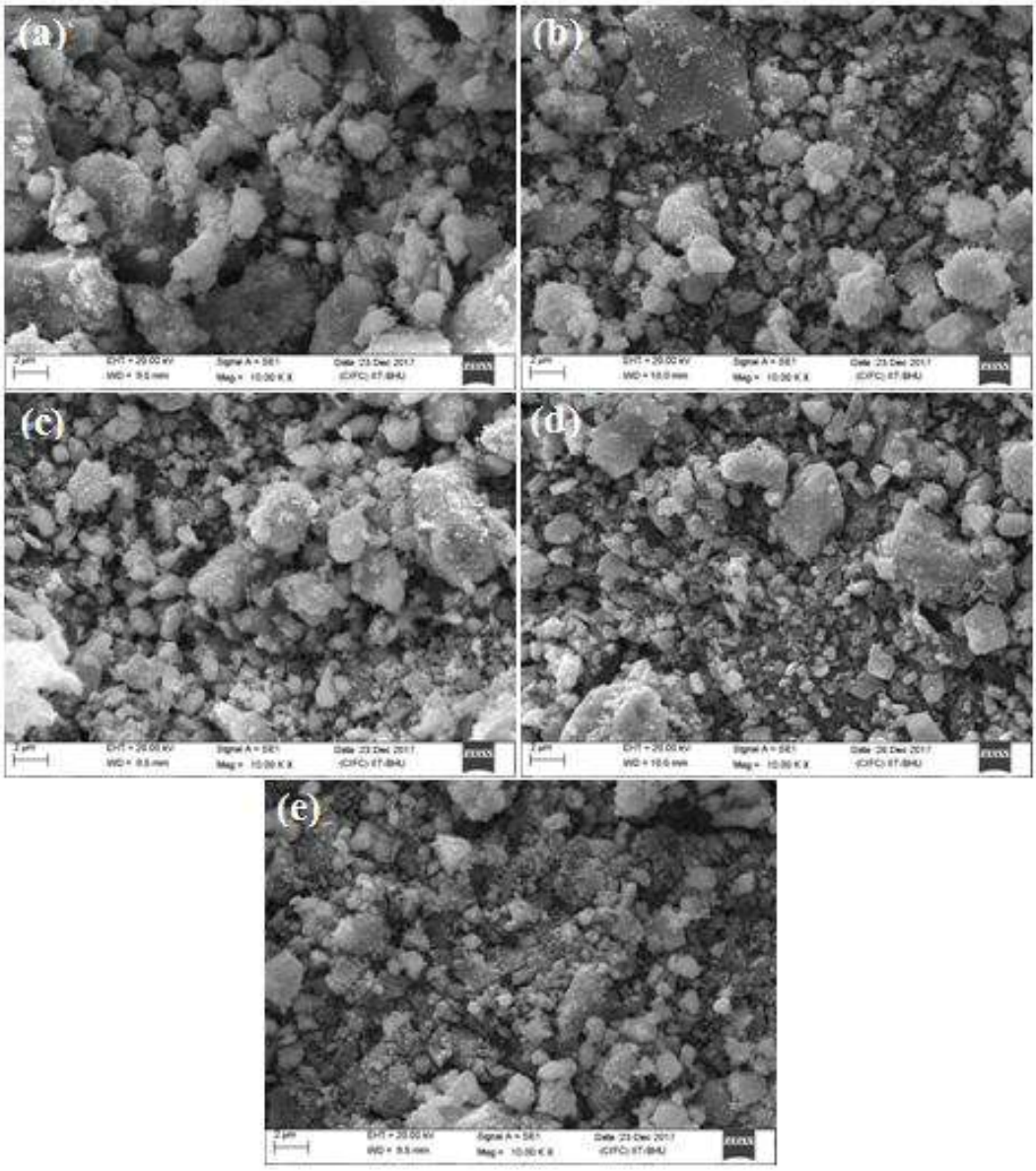

FIGURE 5.6: Scanning electron micrographs of (a)($Fe_{70}Ni_{30}$) (b)($Fe_{70}Ni_{30}$)-2.5ZrO_2 (c)($Fe_{70}Ni_{30}$)-5ZrO_2 (d)($Fe_{70}Ni_{30}$)-10ZrO_2 (e)($Fe_{70}Ni_{30}$)-15ZrO_2 ball milled powders at 10000X magnification.

have a uniform morphology and no agglomeration is there in any of the ball-milled powder. But, the change in morphology with increasing reinforcement concentration is observed. 0 wt.% ZrO_2 containing ball milled powder can be seen having large particles as

compared to other powders. The minimum size of particles with maximum uniformity is observed in 15 wt.% ZrO_2 containing powders. As it is well known that the ZrO_2 particles are very hard as compared to Fe and Ni metal powders. Therefore it is expected that increasing the ZrO_2 particles content has increased the milling efficiency due to their hard nature and helped in reducing the particle size of metal powders.

5.2.2 Microstructure of (Fe-Ni)-ZrO_2 sintered composites

Fig. 5.7 shows the back scattered SEM images of ZrO_2 reinforced sintered composites at 500X magnification. From Fig. 5.7 (a), the presence of small pores (black region) throughout the surface can be seen. Along with these pores, two more regions with different contrast are also observed. The bright contrast region is expected as γ-(Fe,Ni), whereas, the dark region is expected as α-(Fe,Ni) phase.

From Fig. 5.7 (b-e), the small ZrO_2 particles can be observed segregated at the pores and boundary region. Therefore, it can be inferred that these ZrO_2 particles are reducing the pore region by segregating there and improving the microstructure of composite. As the ZrO_2 content is increased, segregation has risen at the boundary region and a very high content of ZrO_2 particles can be observed in the SEM of $(Fe_{70}Ni_{30})$-$15ZrO_2$ composite surface.

Fig. 5.8 (a-e) shows the microstructure of sintered composites at higher magnification (1000X). The presence of pore (black region), α-(Fe,Ni) (dark region) and γ-(Fe,Ni) (bright region) are again observed in the micrographs. Addition of ZrO_2 particles resulted in segregation of these particles at the pore and boundary which is increased by

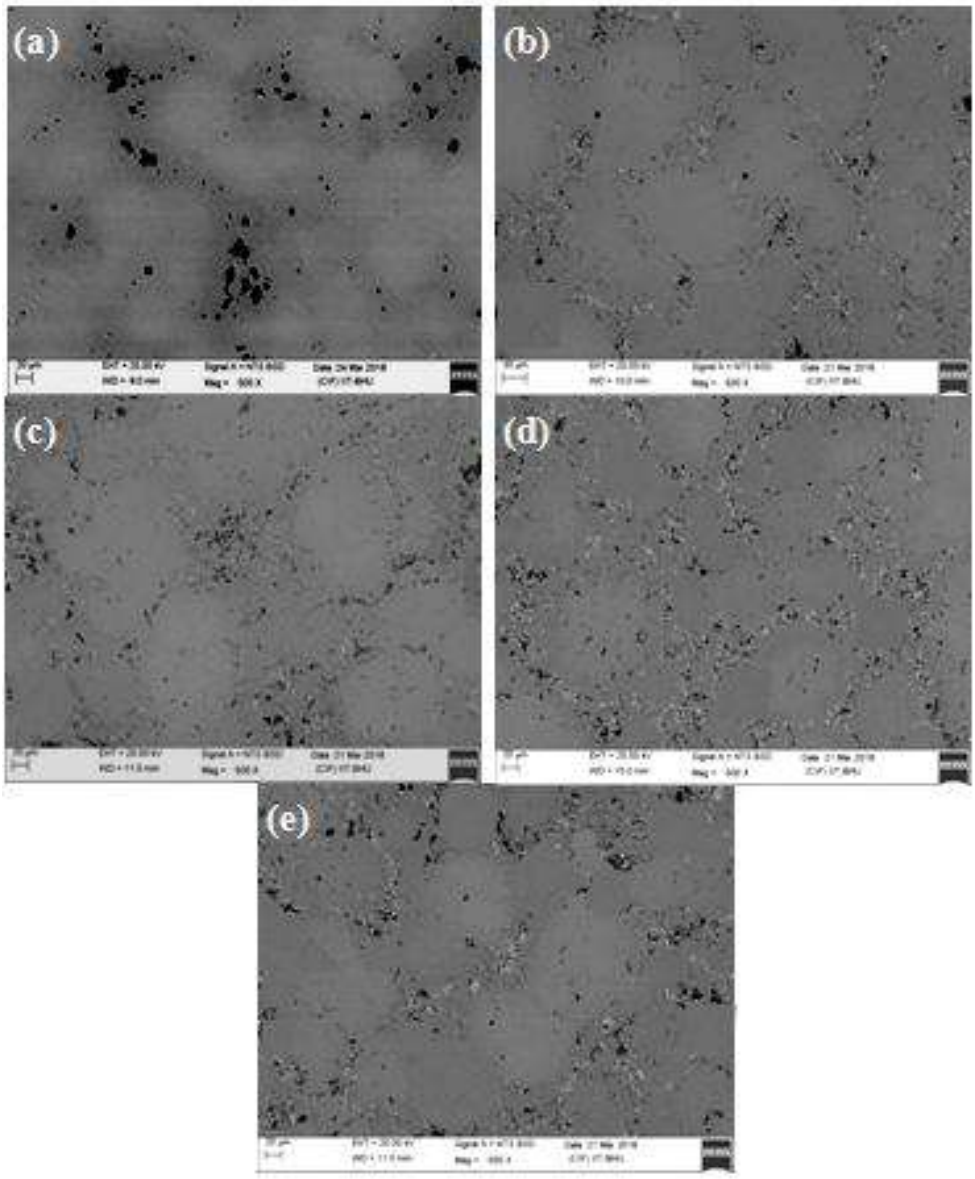

FIGURE 5.7: Backscatterd SEM images of (a)($Fe_{70}Ni_{30}$) (b)($Fe_{70}Ni_{30}$)-2.5ZrO_2 (c) ($Fe_{70}Ni_{30}$)-5ZrO_2 (d) ($Fe_{70}Ni_{30}$)-10ZrO_2 (e)($Fe_{70}Ni_{30}$)-15ZrO_2 sintered composites at 500X magnification.

increasing the ZrO_2 content. The porosity also reduces with increasing ZrO_2 content. Fig. 5.9 shows the composite specimens (a-b) ($Fe_{70}Ni_{30}$)-5ZrO_2 (c-d) ($Fe_{70}Ni_{30}$)-10ZrO_2 (e-f)($Fe_{70}Ni_{30}$)-15ZrO_2 surface microstructures at 10000 and 20000X magnifications. At these higher magnifications, the surface interaction of matrix and reinforced particles can

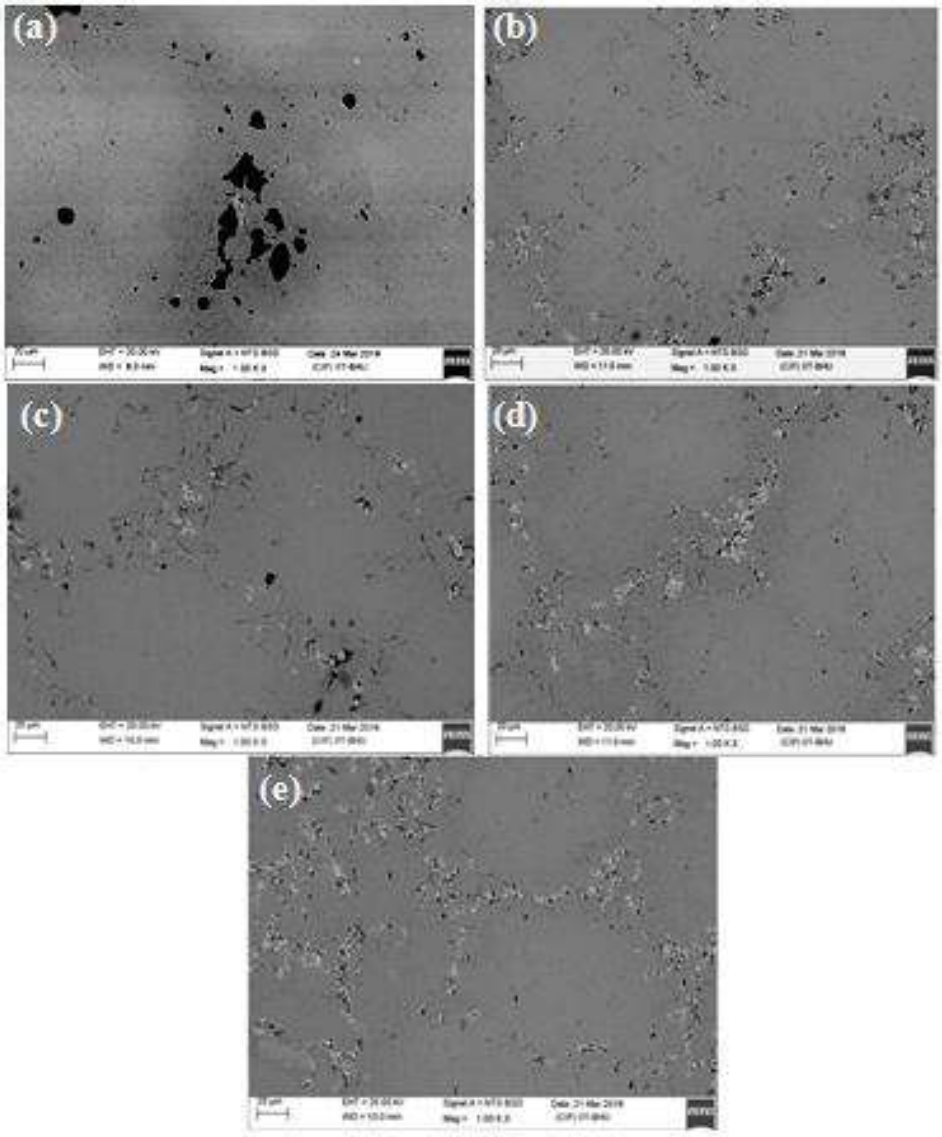

FIGURE 5.8: Backscatterd SEM images of (a)($Fe_{70}Ni_{30}$) (b)($Fe_{70}Ni_{30}$)-2.5ZrO_2 (c) ($Fe_{70}Ni_{30}$)-5ZrO_2 (d) ($Fe_{70}Ni_{30}$)-10ZrO_2 (e)($Fe_{70}Ni_{30}$)-15ZrO_2 sintered composites at 1000X magnification.

be observed. At 5 wt.% and 10 wt.% ZrO_2 concentration, the reinforced particles can be seen embedded properly in the matrix but at 15 wt.%, the crack formation can be observed which is due to increased ceramic-ceramic particle contact and decreased metal-ceramic

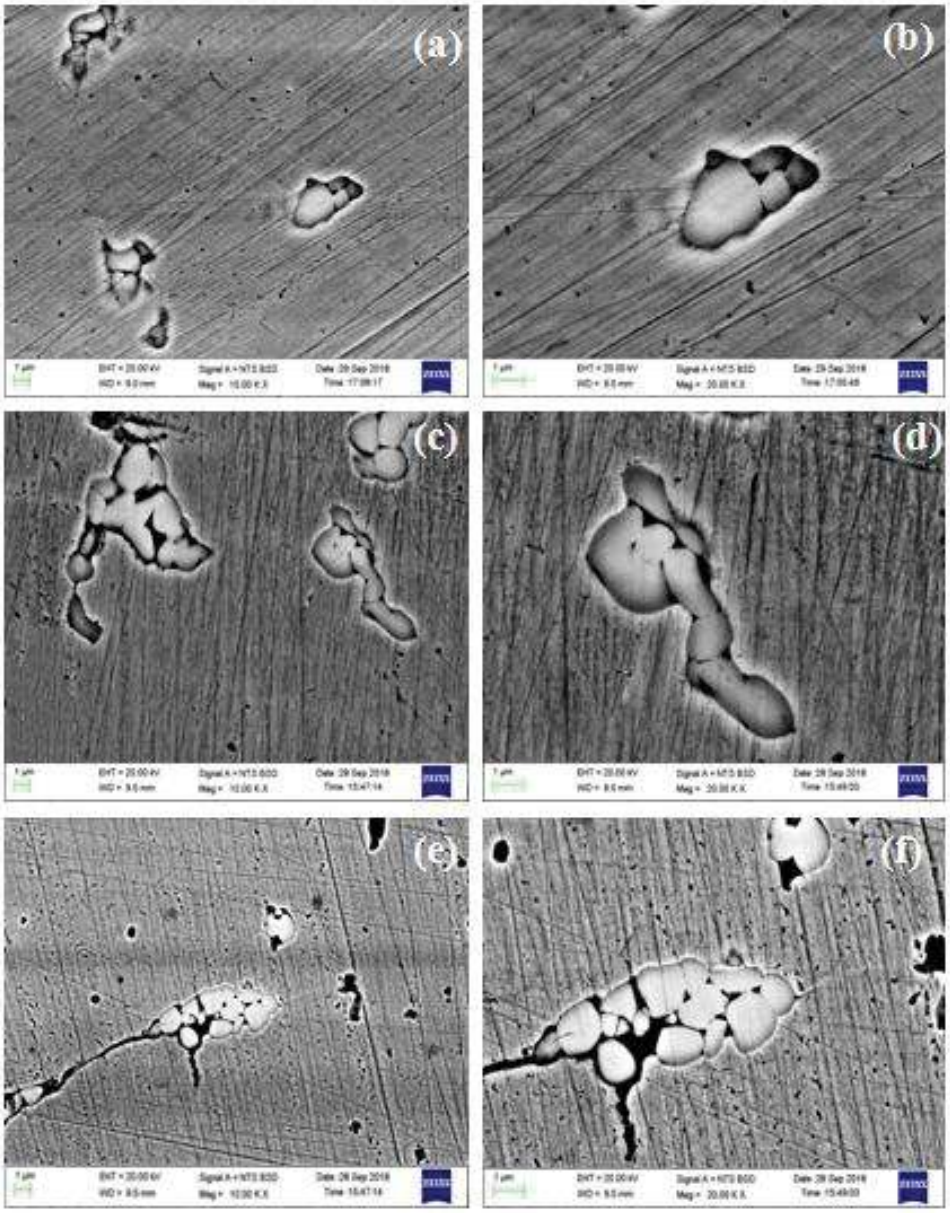

FIGURE 5.9: Backscatterd SEM images of (a-b) $(Fe_{70}Ni_{30})$-$5ZrO_2$ (c-d) $(Fe_{70}Ni_{30})$-$10ZrO_2$ (e-f)$(Fe_{70}Ni_{30})$-$15ZrO_2$ sintered composites at 10000X and 20000Xmagnification.

interaction. These higher ceramic-ceramic particle interaction is helping in the crack formation.

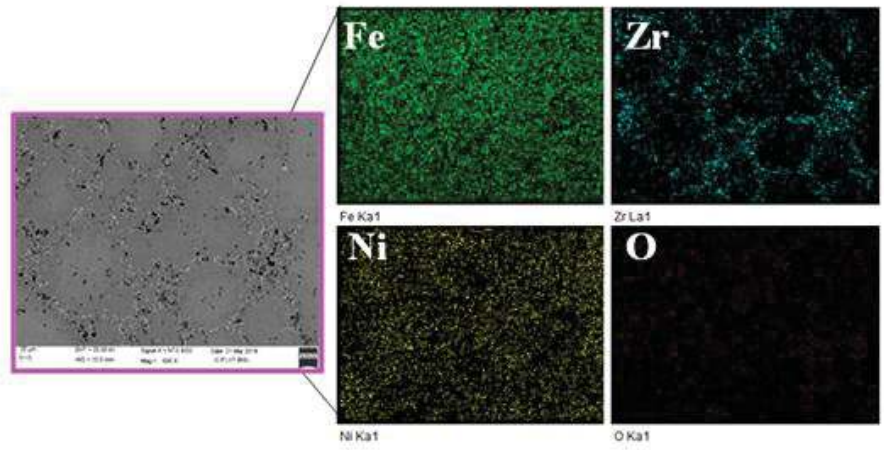

FIGURE 5.10: Elemetal mapping of $(Fe_{70}Ni_{30})$-$10ZrO_2$ composites.

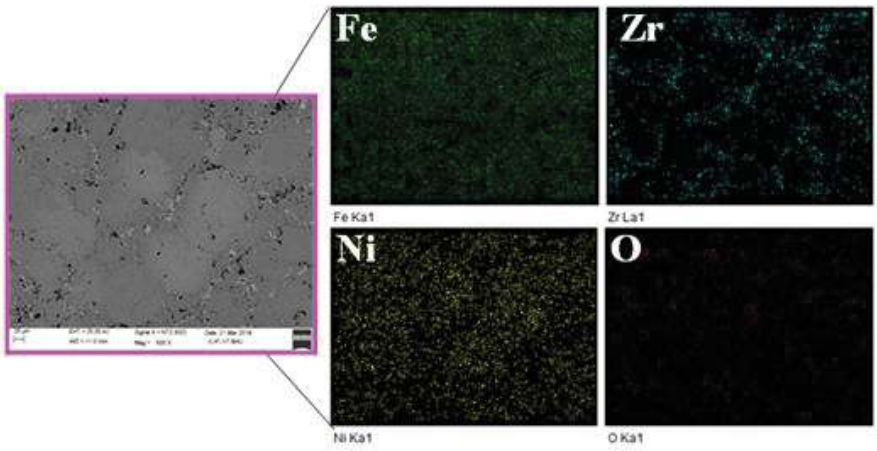

FIGURE 5.11: Elemetal mapping of $(Fe_{70}Ni_{30})$-$15ZrO_2$ composites.

In the metal composites, sintering at higher temperatures (below melting temperature) results in the diffusion of elements which is responsible for phase formation and grain growth. The formation of α and γ(Fe,Ni) is resulting from the inter diffusion of Fe and Ni. Also, the ZrO_2 particles have not formed any intermediate phase with any of the metallic element. It is expected that the nonmetallic particles (ZrO_2) are forced towards the grain boundary during sintering and segregated in the pore region present there.

However, the presence of ZrO_2 particles at grain boundaries help in pore removal during sintering.

Fig. 5.10 and Fig. 5.11 shows the elemental mapping of $(Fe_{70}Ni_{30})$-10ZrO_2 and $(Fe_{70}Ni_{30})$-15ZrO_2 composites, respectively. From the elemental mapping, it can be observed that white particles in the micrograph consist of Zr. Therefore, it is confirmed that the segregated white particles present at the boundary region are ZrO_2 particles. The remaining area has a significant content of Fe and Ni due to the formation of γ and α-(Fe,Ni) phases.

5.3 Density evolution

Fig. 5.12 shows the variation of density of the prepared composites after sintering. It is prominent that the maximum density is achieved in $(Fe_{70}Ni_{30})$ sintered specimen. A decrease in the density is observed when ZrO_2 is added in $(Fe_{70}Ni_{30})$ matrix. From the literature [89], it is well known that the theoretical density of Fe is 7.87 gm/cc, Ni is 8.90 gm/cc and ZrO_2 is 5.85 gm/cc. Therefore, as more and more ZrO_2 particles are added, a decrease in the density is observed. In case of metals, the higher sintering temperature results in elemental diffusion, which improves the solid phase sintering ability. It results in densification and phase formation. In the present work, diffusion between Fe and Ni elements has resulted in α and γ-(Fe,Ni) phase formation. But as mentioned above, ZrO_2 particles have a very high melting temperature and strong ionic bonding, therefore they remained unreacted and did not participate in forming any intermediate phase. However, it has a lower density than the matrix phase thus it contributes in reducing the density of

composite. The density of ($Fe_{70}Ni_{30}$) alloy specimens is $\sim$ 6.35 gm/cm^3. The density of composite specimens with 2.5, 5, 10 and 15 wt.% ZrO_2 are 5.92, 5.76, 5.65 and 5.59 gm/cm^3, respectively. It can be observed that there is a decrement in density with addition of 2.5 wt. % ZrO_2 from 6.34 to 5.92 gm/cm^3. However, further dercrement in density with increasing ZrO_2 content is not much. Thus the addition of ZrO_2 results in more homogenized powder after ball milling and better sintering with reduced porosity. It is also supported by the microstructural observations as described in section 5.2.2.

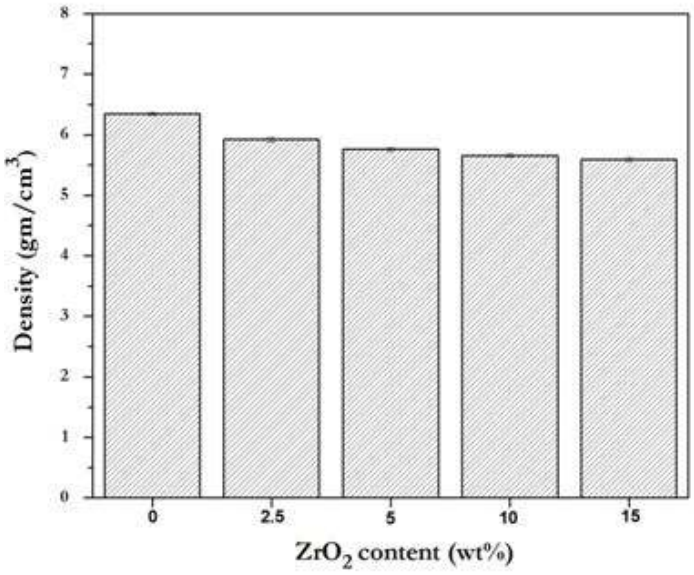

FIGURE 5.12: Density plot of sintered composites with varying ZrO_2 content.

5.4 Hardness

Fig. 5.13 shows the variation of hardness in composites with the increase in ZrO_2 reinforcement content. It is observed that there is an increase in the hardness value with the addition of ZrO_2 particles. The specimen ($Fe_{70}Ni_{30}$) with 0 wt.% ZrO_2 content shows

hardness around 91 Hv. When 2.5 wt.% ZrO_2 particles have been added in ($Fe_{70}Ni_{30}$) composition, the hardness value has increased to 97 Hv. The addition of 5 and 10 wt.% ZrO_2 content resulted in 103 Hv and 108 Hv hardness, respectively. The maximum hardness resulted in 15 wt.% ZrO_2 containing composite with 119 Hv hardness value.

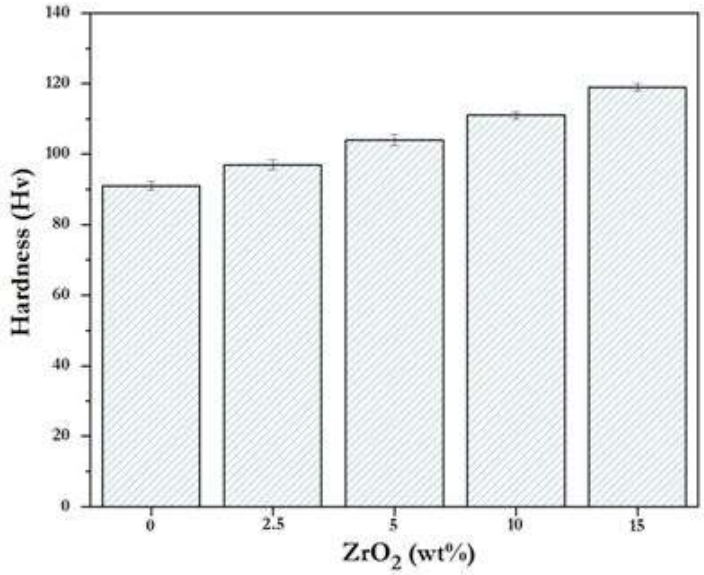

FIGURE 5.13: Hardness plot of sintered composites with varying ZrO_2 content.

For the metal specimen ($Fe_{70}Ni_{30}$), the indentation during hardness measurement results in plastic deformation. Pure alloy specimen shows lower hardness value. The addition of hard ZrO_2 particles retards the plastic deformation and provides the support to the soft metal region during indentation. This results in the higher hardness of ZrO_2 reinforced composites. As ZrO_2 particles concentration is increased, the hardness increased and it is maximum for ($Fe_{70}Ni_{30}$)-15ZrO_2 composite.

5.5 Dry sliding wear properties

The influence of reinforcement content on the wear behavior of composites at different applied loads with fixed sliding speed and sliding distance is shown in Fig. 5.14. Generally, wear loss increases with the increase in applied load for most of the materials. It is well studied that the wear loss in pure metal increases considerably with load, whereas it is comparatively less in case of composites reinforced with hard ceramic particles. In the present work, the addition of ZrO_2 particles as reinforcement phase retards the metal flow, which reduces the material loss during sliding. Therefore, the observed wear rate in the composites is much less as compared to the metal specimens.

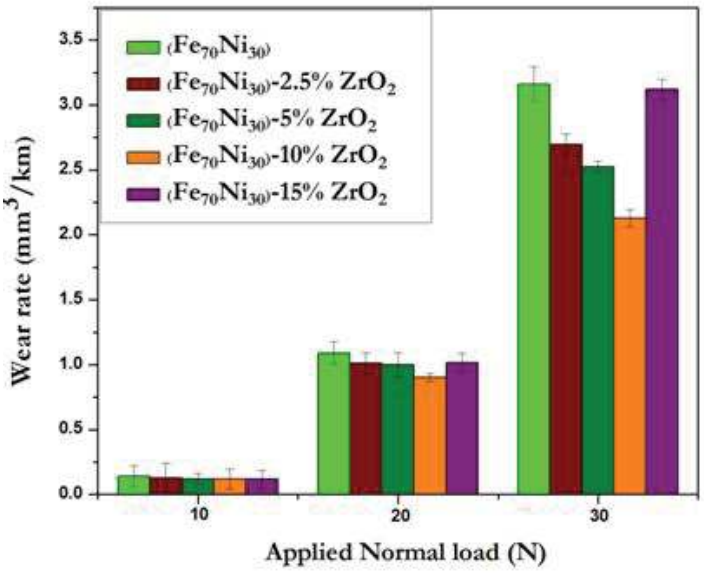

FIGURE 5.14: Wear rate in different specimens at different loads.

At lower applied load, the effect of ZrO_2 concentration is less prominent, whereas it increases significantly at higher applied load. This may be due to the work hardening which is in good agreement with the previous reported studies [121]. In case of metal

matrix composites, generally two types of wear mechanism occur. First is adhesive wear which occurs at lower applied load and results in less material loss. Second is abrasive wear mechanism, which is prominent at higher applied load and results in high material loss [39]. Therefore, in the present case, the material loss has significantly increased at 30N as compared to 10 and 20N.

It is also prominent that the wear rate decreases with increase in ZrO_2 particles concentration. This increase in wear resistance occurs as a result of dispersion strengthening and the good interfacial bond between the metal and the dispersed phase. From the Archard's equation [115, 116], wear loss is inversely proportional to the material's hardness, which could be expressed as Q=kW/H. Here Q is the material removed from the surface, W is normal applied load, H is the surface hardness, and k is wear coefficient. At 10N applied load, the difference in wear rate of composites is not much distinguishable, but at 20 and 30N load, a significant difference in wear rate is observed. For specimen ($Fe_{70}Ni_{30}$), the wear rate is 1.09 mm^3/km at 20N applied load. Addition of ZrO_2 reinforcement resulted in a decrease in wear rate. Wear rate for 2.5, 5 and 10 wt.% reinforced composites is 1.04, 0.99 and 0.90 mm^3/km, respectively. But increasing the reinforcement content up to 15 wt.% resulted in higher wear rate, i.e., 1.03 mm^3/km. A similar trend is again observed at 30N normal applied load. Wear rate of 3.16 mm^3/km is observed for ($Fe_{70}Ni_{30}$) specimen at 30N applied load. Addition of ZrO_2 reinforcement again resulted in decreased wear rate. The wear rate of 2.5, 5 and 10 wt.% reinforced composites is 2.69, 2.52 and 2.12 mm^3/km, respectively. At 15 wt.% reinforcement content, it is observed that the

wear rate again increased to 3.12 mm^3/km. At 15 wt.% reinforcement content, the metal-ceramic interaction becomes weak which makes the composite brittle and high wear rate is observed. At 30N applied load, the abrasive wear mechanism becomes dominant and causes a severe plowing.

Fig. 5.15 shows the coefficient of friction (COF) verses time plot for composite $(Fe_{70}Ni_{30})$-$10ZrO_2$ at 10, 20 and 30N applied loads. In this plot, it can be observed that initially, COF increases sharply with increasing time, and after that it stabilizes at some constant value. COF also increases with increasing applied load. During sliding, increasing the applied load results in a high contact between the moving disc and sample surface. Also, the debris coming out from the specimen surface results in high friction between both the surfaces during the test and hence a high COF value is observed. Samples examined at comparatively higher load results in more debris removal and COF values.

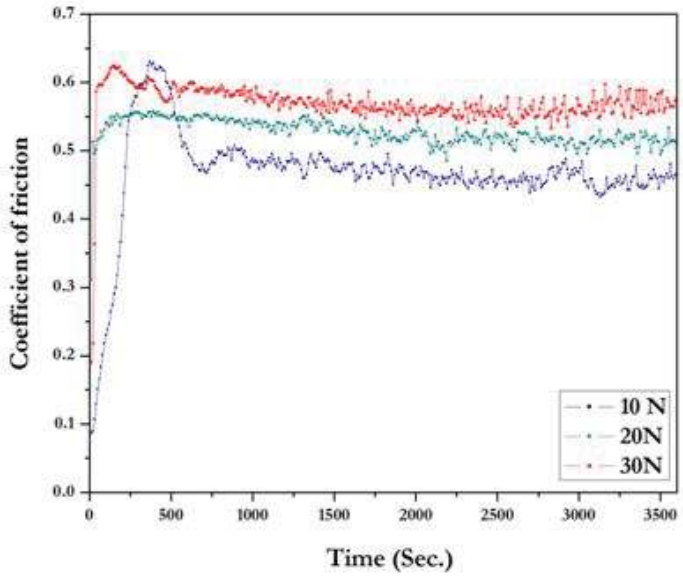

FIGURE 5.15: COF vs. Time plot for the composite $(Fe_{70}Ni_{30})$-$10ZrO_2$ at different loads.

Fig. 5.16 shows the COF versus time plot for different specimens tested at 30N applied load during wear test. It is observed that the COF value for the specimen ($Fe_{70}Ni_{30}$) is around 0.7. As this sample does not contain any reinforcement phase, therefore, the volume loss is more as compared to other ZrO_2 particle reinforced composite specimens. When the debris particles of the surface come between the moving disc and exposed specimen surface, it results in a high COF. In case of composite reinforced with 2.5 wt.% ZrO_2 particles, the COF value has decreased slightly as compared to ($Fe_{70}Ni_{30}$). It is observed that the COF value decreases with increase in ZrO_2 particles up to 10 wt.%. But, in case of 15 wt.% ZrO_2 reinforced composite, COF value again increases with high volume loss. As expected, the ceramic-ceramic particles interaction increases in case of 15 wt.% ZrO_2 reinforced composites and metal-ceramic particle interaction decreases. This attributes to the loosening of reinforcement particles in the composite during sliding.

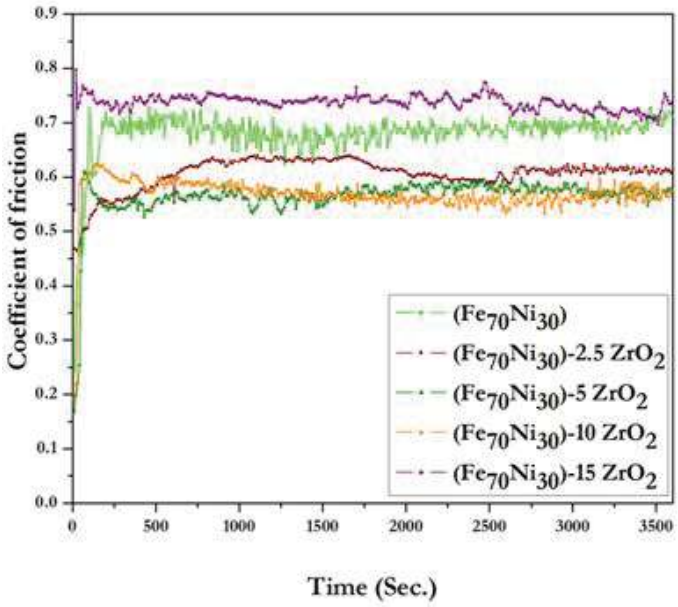

FIGURE 5.16: COF vs. Time plot for different composites at 30N applied load.

Fig. 5.17 shows the SEM images of worn surfaces of ($Fe_{70}Ni_{30}$) and ZrO_2 reinforced composites under 10-30N normal applied load. The worn surface of ($Fe_{70}Ni_{30}$) specimen (Fig. 5.17 a) without ZrO_2 reinforcement shows slight grooves at lower load, i.e., 10N, which are present along the sliding direction. At higher applied load (i.e., 20 and 30N), plastic deformation and grooves are observed, which may be due to the frictional heat generated during sliding. The material removal by plowing (occurs to sideways of grooves to form ridges adjacent to grooves) is also evident from the micrographs. The worn surface micrograph of 2.5% ZrO_2 reinforced composites show the narrow grooves and less material loss as compared to the pure metal surface (Fig. 5.17 b). Increasing the ZrO_2 fraction up to 10% reduces both the depth of grooves and material loss (Fig. 5.17 c-d). It is evident that the hard ceramic particles inhibit the plastic deformation during sliding, which results in less material loss. Although the hardness of a composite is widely used parameter for evaluating wear resistance, it is not always a key factor thus it is not always a reliable approach. It is reported in previous studies that wear resistance also depends upon the toughness of material which reduces with increasing hardness [115, 117].

Even though increasing the reinforcement phase helps in reducing the wear rate, but when the ZrO_2 concentration is very high (i.e., 15 wt.%), the wear rate has increased dramatically at higher load (20 and 30N). This decrease in wear resistance may be due to the increased contact between ceramic to ceramic particles, which decrease the bond strength between the metal and dispersed phase and makes the composite brittle during synthesis. At 15% reinforcement, adhesive wear became more prominent due to ceramic particle removal during repeated sliding, and thus a very high wear rate has occurred [122]. At

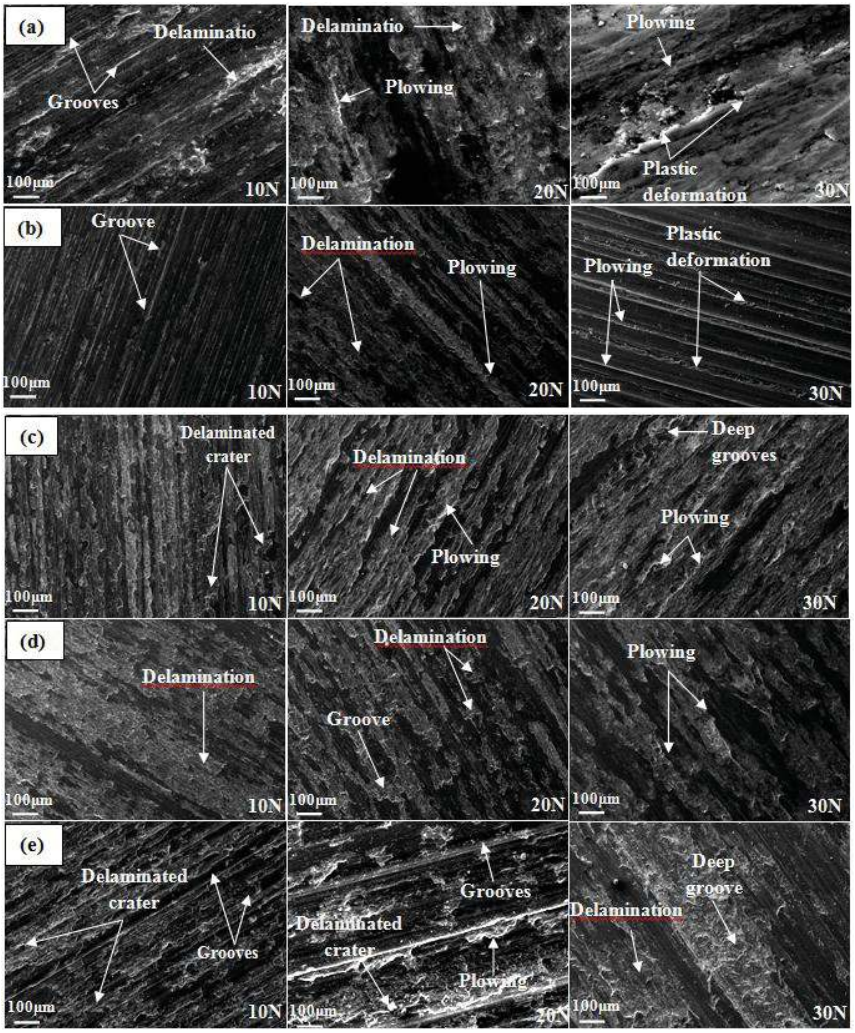

FIGURE 5.17: Worn surface SEM micrographs of (a)($Fe_{70}Ni_{30}$) (b)($Fe_{70}Ni_{30}$)-2.5ZrO_2 (c) ($Fe_{70}Ni_{30}$)-5ZrO_2 (d) ($Fe_{70}Ni_{30}$)-10ZrO_2 (e)($Fe_{70}Ni_{30}$)-15ZrO_2 composites.

higher load conditions, the removal of hard particles from the surface increases, which come in between the disc and material surface and resulted in the seizure of matrix phase. SEM images illustrated the deep grooves and craters on the surface of the composite containing 15% ZrO_2 (Fig. 5.17 e).

5.6 Electrochemical Behavior

5.6.1 Potentiodynamic polarization Measurements

The electrochemical behavior of the prepared specimens was investigated by potentiodynamic polarization measurement using Tafel extrapolation technique. The kinetics of the corrosion reaction can be obtained from the shape of polarization curves. The polarization curves for different synthesized specimens were recorded after 1h of electrode immersion in 3.5 wt.% NaCl solution at room temperature (Fig. 5.18). Obtained polarization curve is similar for the ZrO_2 reinforced composites to that of pure Fe and the ($Fe_{70}Ni_{30}$) system. It is also observed from the plots that the polarization curves for pure iron shows most negative corrosion potential -739 mV. The addition of Ni and ZrO_2 results in shifting the corrosion potential towards more positive values. Maximum positive value is observed for 10% ZrO_2 containing composite.

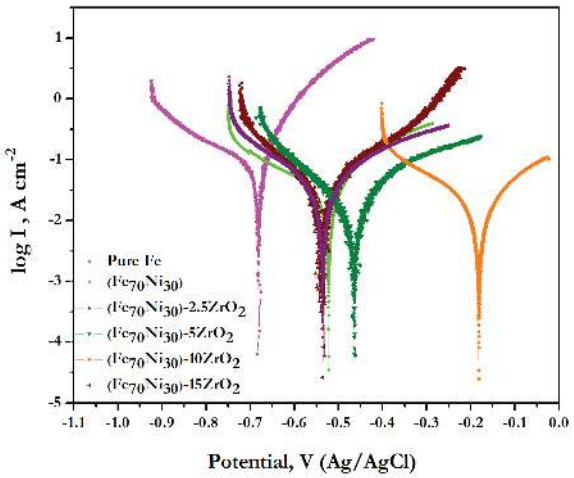

FIGURE 5.18: Tafel plots of composites examined in 3.5%NaCl solution.

TABLE 5.1: Electrochemical parameters obtained from potentiodynamic polarization curves.

S.No.	Specimen Name	$E_{corr}(mV)$	$I_{corr}(\mu A/cm^2)$	C_r(mpy)	$\mu_p\%$
1	Pure Fe	-739	108.3	118.12	-
2	$(Fe_{70}Ni_{30})$	-558	36.30	41.43	66.51
3	$(Fe_{70}Ni_{30})$-2.5ZrO_2	-567	32.29	41.00	70.21
4	$(Fe_{70}Ni_{30})$-5ZrO_2	-513	26.39	35.41	75.65
5	$(Fe_{70}Ni_{30})$-10ZrO_2	-190	19.69	28.39	81.83
6	$(Fe_{70}Ni_{30})$-15ZrO_2	-567	37.30	57.29	65.59

The electrochemical parameters, i.e., corrosion potential (E_{corr}) and corrosion current density (I_{corr}) were obtained from the extrapolation of linear Tafel segments of cathodic and anodic lines of the polarization curves. The values of corrosion rate (C_r) and protection efficiency (μ_p) [38] were calculated from the obtained I_{corr} value using the equation given below and listed in Table. 5.1.

The calculation of corrosion rate (C_r) and protection efficiency (μ_p) was done by using the obtained I_{corr} value [11] given below:

$$C_r(mpy) = \frac{0.13 I_{corr}(E.W.)}{d} \tag{5.1}$$

$$\mu_p\% = \left(\frac{I^o_{corr} - I^i_{corr}}{I^o_{corr}}\right) \times 100 \tag{5.2}$$

Where mpy is milli-inches per year, I_{corr} is corrosion current density (μA/cm^2), E.W. is equivalent weight (g), d is density (g/cm^3), and I°corr and I^icorr are corrosion current densities of pure iron and composite specimens, respectively.

On comparing the data recorded in Table. 5.1, it is observed that the corrosion current density value decreases for the $(Fe_{70}Ni_{30})$ system and other ZrO_2 reinforced composites as compared to pure Fe. The corrosion resistance of the composite specimens is found

to improve with increasing the reinforcement content up to 10 %, i.e., the minimum I_{corr} value is recorded for this composition. The primary corrosion reactions for the ($Fe_{70}Ni_{30}$) system in 3.5% NaCl solution is supposed due to the present iron-rich phase in the material. In the literature, it is reported that Ni can resist corrosive action of Cl^- ions [119,123] due to the possible formation of Fe-Ni alloy phases, which are not easily attacked by the Cl^- ions. In the present system, the addition of Ni to Fe leads to the formation of γ-(Fe,Ni) and shows better corrosion resistance towards NaCl medium. Consequently, the dissolution process of Ni to Ni^{2+} ions in NaCl is slow and hence the corrosion process on the ($Fe_{70}Ni_{30}$) surface is mainly due to the dissolution of iron-rich phase. The influence of Cl^- ions on the corrosion rate of iron sample can be interpreted as a balance between two processes competing on the metal surface, stabilization of the protective film by OH^- adsorption and disruption of the film by Cl^- ions adsorption. When the activity of chlorides overcomes that of hydroxyl, corrosion occurs. The accepted corrosion mechanism of the iron sample in 3.5% NaCl solution can be suggested in the following sequence [118]:

1. Anodic dissolution of Fe,

$$Fe \rightarrow Fe^{+2} + 2e^- \tag{5.3}$$

$$Fe + OH^- \rightarrow FeOH^-_{ads} \tag{5.4}$$

$$FeOH^-_{ads} \rightarrow FeOH_{ads} + e^- \tag{5.5}$$

$$FeOH_{ads} + OH^- \rightarrow Fe(OH)_2 + e^- \tag{5.6}$$

$$Fe(OH)_2 + OH^- \rightarrow FeOOH + H_2O + e^- \tag{5.7}$$

2. and/or

$$Fe + Cl^- \rightarrow FeCl_{ads} + e^- \tag{5.8}$$

$$FeCl_{ads} \rightarrow FeCl^+_{aq} + e^- \tag{5.9}$$

3. And the cathodic reaction is, reduction of molecular oxygen:

$$O_2 + 2H_2O + 4e^- \rightarrow 4OH^- \tag{5.10}$$

In case of composite specimens, the corrosion current density decreases from 36.30 $\mu A/cm^2$ for ($Fe_{70}Ni_{30}$) system to 26.39 $\mu A/cm^2$ for 5% ZrO_2 reinforced composite. Corrosion current density further decreases to 19.69 $\mu A/cm^2$ for 10% ZrO_2 reinforcement containing composite. This improvement in the performance of the composite materials may be due to the incorporation of the ZrO_2 particles in the metal matrix. It is assumed that the addition of inert oxide (ZrO_2) as a reinforcement diminish the density of active sites on the metal surface and the amount of these active sites further decreases with increasing ZrO_2 content. The improved performance of a metal or alloy due to the incorporation of non-metallic particles is reported in case of coating materials [124]. It is believed that the metal surface possesses defects, gaps, crevices and holes and the ZrO_2 particles fill these defects, slowing down the dissolution of the metal through these active sites. During the initial oxidation period, a protective iron hydroxide layer is formed which becomes more and more compact with an increase in zirconia content and consequently the corrosion resistance against the attack of Cl^- ion is improved. However, in

case of 15% ZrO_2 reinforcement, it is observed that the I_{corr} becomes more. This may be because, at higher concentration of the ZrO_2, the microstructure becomes weak at the grain boundaries, and electrolyte gets space to penetrate at the metal/ reinforcement interface and enhances the corrosion process. Therefore, 10% of ZrO_2 has been found as the optimum concentration for reinforcement in ($Fe_{70}Ni_{30}$) metal matrix.

5.6.2 Electrochemical Impedance Spectroscopy Analysis (EIS)

EIS is a potent technique to be used to get a quantitative evaluation of the corrosion properties of the system that may be difficult using conventional potentiodynamic polarization technique. The detailed information of the corrosion processes at the electrode-electrolyte interface can be obtained by interpretation of the EIS data with an appropriate equivalent circuit (EC). The biggest advantage of EIS technique is that it does not appear to accelerate the corrosion reaction and can also be conducted in situ nondestructively [125]. EIS measurements have been carried out for pure Fe, ($Fe_{70}Ni_{30}$) system and the ZrO_2 reinforced composites.

Fig. 5.19 shows the Nyquist plots for specimens (a) pure iron and $Fe_{70}Ni_{30}$ alloy specimens and (b) $Fe_{70}Ni_{30}$-ZrO_2 composites in 3.5 wt.% NaCl solution. It can be seen that the obtained impedance responses significantly changed for the ($Fe_{70}Ni_{30}$) system and ZrO_2 reinforced composites from that of the pure iron sample. The impedance spectra of pure Fe consist of a single capacitive semicircle showing that the corrosion process is controlled mainly by the charge transfer. However, in case of ($Fe_{70}Ni_{30}$) system one very small capacitive loop is observed at high frequency followed by a big capacitive loop

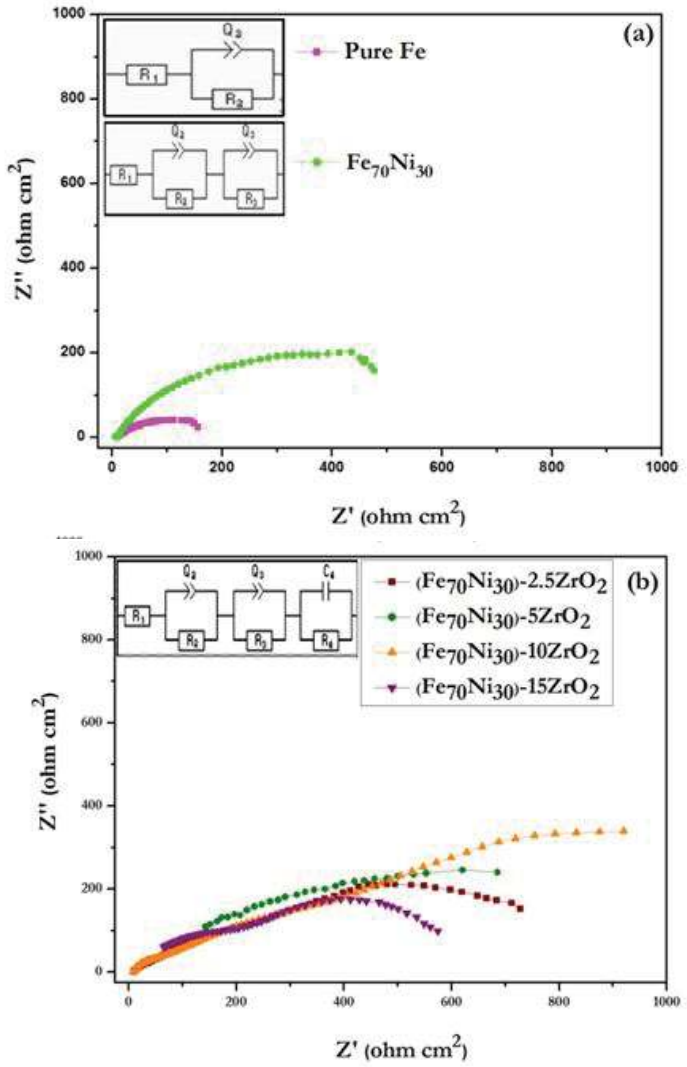

FIGURE 5.19: Nyquist plots obtained for (a) pure Fe and ($Fe_{70}Ni_{30}$), and (b) (Fe,Ni)-ZrO_2 reinforced composites in 3.5 % NaCl. (The equivalent circuit is shown in the inset).

(Fig. 5.19 a). It is seen that the diameter of the semicircle for the ($Fe_{70}Ni_{30}$) system is much larger than that of pure Fe suggesting that the ($Fe_{70}Ni_{30}$) specimen is more corrosion resistant than that of pure Fe. The EIS data has been fitted to appropriate equivalent circuits to properly interpret the results [126,127]. The EC for pure Fe is shown as an inset in Fig. 5.19 (a) which contains one pure resistive part (R_1) that represents the resistance

between working and the reference electrode. This is in series with Q_2, the constant phase element (CPE), which represents the capacitance in parallel with a resistance (R_2). This is for the charge transfer process of the electrode in the electrolyte system. The EC for the ($Fe_{70}Ni_{30}$) alloy system is shown as an inset in the same Fig. 5.19 (a). This circuit contains one additional CR circuit which is in series with the circuit shown for pure Fe. The additional capacitance and resistance for the alloy system may be due to the presence of another phase in the alloy. In the XRD results (Fig. 5.3), it has already been discussed that the ($Fe_{70}Ni_{30}$) specimen contains γ-(Fe,Ni) phase in addition to α-(Fe)/α-(Fe,Ni) and thereby the electrolyte faces two types of grains at the electrode surface.

The impedance spectra for the ZrO_2 reinforced composite specimens show three capacitive loops (Fig. 5.19 b) which are attributed to the charge transfer process of the specimen (electrode)/electrolyte interface, which can be related to changes in the surface due to the formation of composite materials. The EC for the composite specimens comprises three CR circuit. Unlike ($Fe_{70}Ni_{30}$), the third CR circuit for the composite specimens may be due to the presence of ZrO_2 reinforcement in the metal matrix. The ZrO_2 particles are embedded in the host matrix and block the transition path of the charge carrier to the electrode system, which means the active sites for the corrosion process are blocked. Accordingly, it is noted that the diameters of the semicircles have increased for the composite materials than that of pure Fe and ($Fe_{70}Ni_{30}$) specimens. It shows that the composite material is more corrosion resistant as compared to pure Fe and ($Fe_{70}Ni_{30}$) specimens. The increase in the concentration of the reinforcement in the composite material further increases the resistance of the material up to 10%. This may be because the increase in the

concentration of the zirconia causes the increase in the number of the blocking the active sites for the corrosion process. However, a further increase in the concentration of reinforcement caused the decrease in the diameter of the semicircle. This suggests that 10% is the optimum reinforcement concentration to prepare a corrosion resistant material.

5.6.3 Microstructure study after corrosion

Fig. 5.20 (a-f) shows the SEM micrographs of the corroded surfaces after potentiodynamic polarization measurements in NaCl solution. After corrosion test, it has been observed that the surface of the pure iron specimen has been affected maximum among all the prepared specimens. In ($Fe_{70}Ni_{30}$) surface, the formation of γ has contributed in resisting

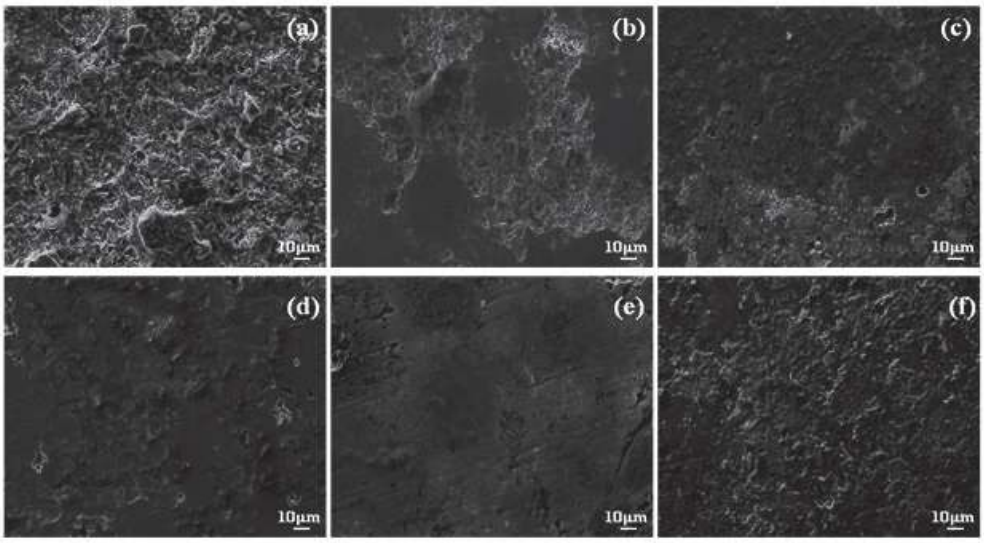

FIGURE 5.20: SEM micrographs of (a) Pure Fe (b)($Fe_{70}Ni_{30}$) (c)($Fe_{70}Ni_{30}$)-2.5ZrO_2 (d) ($Fe_{70}Ni_{30}$)-5ZrO_2 (e) ($Fe_{70}Ni_{30}$)-10ZrO_2 (f)($Fe_{70}Ni_{30}$)-15ZrO_2 composites.

corrosion at the surface. The material surfaces, where γ phase forms are mostly corrosion resistant. Rest of the matrix, where α phase forms, is mostly attacked by corrosion. It can be seen from Fig. 5.20 (b). ZrO_2 reinforcement has played a significant role in the

composite specimens. Increasing ZrO_2 content from 2.5 to 10 % in ($Fe_{70}Ni_{30}$) matrix, corrosion resistance is improved, which is evident from the Tafel plots and impedance data. Thus, the electrolyte does not attack the specimen surface. From microstructural analysis, it is found that ($Fe_{70}Ni_{30}$)-10ZrO_2 is the least affected surface (Fig. 5.20 e) due to corrosion. Above 10% reinforced composite, interface region of metal and ceramic has become week, which is responsible for the brittleness in the material. This weak region has allowed the electrolyte to pass through and the value of corrosion current has increased. Therefore the surface of ($Fe_{70}Ni_{30}$)-15ZrO_2 has been affected most in comparison to all other synthesized composite specimens.

5.7 Summary of the chapter

The present chapter has been focused on the sintering, mechanical and corrosion behavior of (Fe,Ni)-ZrO_2 sintered composites. The effect of ZrO_2 particles concentration on both the ball milled powders and sintered specimens is analyzed. The current work has been done to investigate the effect of ZrO_2 as ceramic reinforcement on the tribological and corrosion behavior of iron-nickel matrix based composites. The concluding remarks of work done are as follows:

1. The novel ($Fe_{70}Ni_{30}$)-ZrO_2 composites have been prepared successfully using powder metallurgy route. The phase study has evident the formation of γ and α-(Fe,Ni) phases in the ($Fe_{70}Ni_{30}$) matrix. Distinct ZrO_2 reinforced particles were observed in composites from XRD and microstructure analysis. There was no evidence of

the in-situ intermediate phase formation between reinforcement and matrix phases in any of the composites.

2. Addition of ZrO_2 in ($Fe_{70}Ni_{30}$) matrix has contributed to improving the wear resistance by supporting the matrix phase, which reduced the material loss during sliding. An increase in reinforcement fraction up to 10% resulted in the increase in wear resistance. Above this content, the composite has shown a brittle nature which resulted in the removal of hard reinforcement particles during sliding, which was also observed in the SEM micrographs. These particles when came in between the surface of disc and composite caused the formation of deep grooves and high material loss as a result of abrasive wear. Therefore the wear resistance of ($Fe_{70}Ni_{30}$)-15ZrO_2 was found to be reduced dramatically.

3. The improvement in corrosion resistance was observed due to the presence of both γ-(Fe,Ni) and ZrO_2 reinforcement phases. The γ phase remains fixed in all the composites due to the fixed matrix composition. Therefore, it has helped in improving the corrosion resistance up to the certain content. Addition of ZrO_2 particles into the matrix phase resulted in enhancement of the corrosion resistance. The maximum protection efficiency of 82% was achieved for ($Fe_{70}Ni_{30}$)-10ZrO_2 composite with the minimum corrosion current value (i.e 19.69 μA/cm^2). Above 10% reinforcement content, the increase in corrosion current and degradation in the protection efficiency is observed. It can be correlated with the brittleness in the composite at a high ZrO_2 concentration. The effect of corrosion on the different composite

surfaces was also observed using surface study (SEM) which has shown a good agreement with the obtained instrumental data.